

Scale Dependencies and Self-Similarity Through Wavelet Scattering Covariance

R. Morel, G. Rochette, R. Leonarduzzi, J.-P. Bouchaud, S. Mallat

Abstract—We introduce a scattering covariance matrix which provides non-Gaussian models of time-series having stationary increments. A complex wavelet transform computes signal variations at each scale. Dependencies across scales are captured by the joint covariance across time and scales of complex wavelet coefficients and their modulus. This covariance is nearly diagonalized by a second wavelet transform, which defines the scattering covariance. We show that this set of moments characterizes a wide range of non-Gaussian properties of multi-scale processes. This is analyzed for a variety of processes, including fractional Brownian motions, Poisson, multifractal random walks and Hawkes processes. We prove that self-similar processes have a scattering covariance matrix which is scale invariant. This property can be estimated numerically and defines a class of wide-sense self-similar processes. We build maximum entropy models conditioned by scattering covariance coefficients, and generate new time-series with a microcanonical sampling algorithm. Applications are shown for highly non-Gaussian financial and turbulence time-series.

Index Terms—maximum entropy, non-Gaussianity, scattering, self-similarity, time-series, wavelets.

I. INTRODUCTION

Time-series having stationary increments with variations on a wide range of scales are encountered in physics, finance, biology, medicine and many other fields. They typically include complex intermittent phenomena with local burst of activity, and time-asymmetries due to some form of causality. The importance of this topic was first recognized by Mandelbrot [1]–[3] and lead to a considerable body of work on multifractal signals [4]–[10]. Among multi-scale processes, self-similar models have a probability distribution which is invariant to scaling, up to multiplicative factors. To validate numerically such models, it is necessary to introduce weaker forms of self-similarity that can be estimated over limited time-series.

Simplified multi-scale models have first been defined from marginal distributions of signal increments, by Frisch and Parisi [11]. A weak form of self-similarity is a scaling invariance of high-order moments of these marginal distributions. This can be sufficient to detect non-Gaussian distributions. Section II reviews these models together with the multifractal formalism, which replaces increments by wavelet coefficients. Marginal distributions at each scale are simple to estimate, but they do not capture dependencies of signal variations across scales. These dependencies are crucial to specify many properties, and particularly the existence of transient events, which have particular signatures at multiple scales. The central result of this paper is the construction of a scattering covariance which specifies these dependencies. Its diagonal approximation provides a parcimonious, low-dimensional representation

of scale interactions, which we use to define generative models of multi-scale processes.

A wavelet transform computes multi-scale signal variations. Section III-B proves that wavelet coefficients are nearly uncorrelated at different scales, because their phases oscillate at different frequencies. To measure non-linear dependencies across scales, it is tempting to move towards higher order moments [12]. This requires to compute many moments with high variance estimators, which gives poor numerical results over limited size time-series. Lower variance estimators have been studied by replacing high-order moments with phase harmonics [13] or by eliminating the phase with a modulus non-linearity [14], [15]. We show that scale dependencies can be represented by correlating wavelet coefficients and their modulus. We prove that self-similar processes yield normalized correlation matrices which are invariant to scaling. Section IV derives a definition of wide-sense self-similarity, which is analogous to the definition of wide-sense stationarity, where invariance to translation of covariance matrices is replaced by an invariance to scaling.

Wavelet modulus cross-correlation matrices are too large to be estimated accurately from a single time-series realization. Section V shows that applying a second wavelet transform defines a scattering covariance matrix which is nearly diagonal. Dependencies across scales are captured by diagonal scattering cross-correlation coefficients, also called scattering cross-spectrum, which can be estimated from a single realization. We shall see that scattering covariances provide an interpretable dashboard which captures non-Gaussian properties, including burst of activity and time-asymmetries, as well as self-similarity.

Fractional Brownian motions, Poisson processes, multifractal random walks and Hawkes processes are often used as models of multi-scale processes which may or may not be self-similar. Section VI shows that the scattering covariance reveals their specific properties. By analyzing the scattering covariance of S&P financial time-series and turbulent jets, we show that none of the mathematical models presented captures all properties of these complex time-series.

Section VII defines maximum entropy models conditioned by scattering covariance values. We generate time-series according to these models with the microcanonical sampling algorithm in [16]. We show that these generative models can approximate fractional Brownian motions, multifractal random walks and Hawkes processes but also S&P financial time-series or turbulent jets.

Notations: We write M^* the adjoint and hence the complex conjugate of the transposed matrix M . We denote $\hat{x}(\omega)$ the Fourier transform of $x(t)$.

II. SELF-SIMILARITY THROUGH MULTI-SCALE MARGINAL DISTRIBUTIONS

We consider random processes $X(t)$ whose increments are stationary. Self-similarity and multifractal properties have first been studied by analyzing the marginal distributions of increments, and from wavelet coefficients. The next two sections review important properties of these marginal distributions, before considering dependencies across scales.

A. Self-Similarity of Increments

If $X(t)$ is stationary then its increments are stationary but the reverse is not always true. If X has stationary increment, $\mathbb{E}\{X(t)\}$ and $\mathbb{E}\{X^2(t)\}$ may depend on t , as for a Brownian motion [17]. The increment of a random process $X(t)$ at a scale $2^j \in \mathbb{R}^+$ for $j \in \mathbb{R}$ is written

$$\delta_j X(t) = X(t) - X(t - 2^j).$$

We suppose that $\delta_j X$ is stationary for any $j \in \mathbb{R}$. It is said to be self-similar [18] up to a maximum scale 2^J if for all $\ell \geq 0$ there exist real random variables A_ℓ which are log infinitely divisible and independent of X such

$$\left\{ \delta_j X(t) \right\}_{j \leq J, t \leq T} \stackrel{d}{=} A_\ell \left\{ \delta_{j-\ell} X(2^{-\ell} t) \right\}_{j \leq J, t \leq T}. \quad (1)$$

This equality is in distribution, which means that joint probability distributions of random variables on the left and right hand-sides are equal for any (j_1, \dots, j_n) and (t_1, \dots, t_n) with $n > 0$. Increments thus have joint distributions which are invariant to dilation, up to random multiplicative factors. The maximum scale 2^J may be fixed. In this case, we assume that $X(t)$ and $X(t - \tau)$ are nearly independent for $\tau \gg 2^J$. It results that X is stationary and 2^J is called the *integrable scale*. However, a process X may also be defined as a limit when J goes to ∞ in which case X may be non-stationary, as in the Brownian motion case.

The self-similarity definition (1) is very restrictive, often not satisfied, and impossible to verify numerically over high-dimensional time-series. Since increments $\delta_j X(t)$ are stationary, their marginal probability distribution for t fixed does not depend upon t . A weak form of self-similarity is obtained from the scaling properties of these marginal distributions. Frisch and Parisi [11] proposed to do so through moments $\mathbb{E}\{|\delta_j X(t)|^q\} < \infty$ for $q \in \mathbb{R}$. Since A_ℓ is infinitely divisible, Appendix A shows that the self-similarity definition (1) implies that for all $q \in \mathbb{R}$ there exists ζ_q such that

$$\mathbb{E}\{|\delta_j X(t)|^q\} = \tilde{c}_q \mathbb{E}\{|A_j|^q\} = \tilde{c}_q 2^{j\zeta_q}. \quad (2)$$

If X is Gaussian then one can verify that ζ_q is linear in q . It results that any non-linear dependency of ζ_q as a function of q implies that X is not Gaussian. This was initially proposed by Kolmogorov to detect non-Gaussian properties in turbulent flows.

Processes having stationary increments have a generalized power spectrum $P_X(\omega)$, which is mathematically defined from the Fourier transform of the autocorrelation of increments, to avoid issues related to the non-stationarity of X [17]. The scale invariance (2) of moments for $q = 2$ implies that this

power spectrum is also scale invariant and has a power-law decay specified by ζ_2 [17]

$$P_X(\omega) = c_2 |\omega|^{-\zeta_2 - 1}. \quad (3)$$

For $\zeta_2 \geq 0$, the divergence of $P_X(\omega)$ at low frequencies is responsible for the non-stationarity of X .

B. Wavelet Transform Marginals

Similarly to increments, a wavelet transform computes the variation of X at all scales 2^j . However, it relies on wavelets ψ that are well localized in the Fourier domain, as opposed to Diracs used to compute pointwise increments. The multifractal formalism [7] shows that this property is needed in order to specify pointwise regularity properties of $X(t)$. We briefly review the main properties of wavelet transforms.

A wavelet $\psi(t)$ has a fast decay away from $t = 0$, and a zero-average $\int \psi(t) dt = 0$. We normalize $\int |\psi(t)| dt = 1$. The wavelet transform computes the variations of a signal x at each scale 2^j with

$$Wx(t, j) = x \star \psi_j(t) \quad \text{where} \quad \psi_j(t) = 2^{-j} \psi(2^{-j} t). \quad (4)$$

If $\psi = \delta(t) - \delta(t - 1)$ then we recover the signal increments $WX(t, j) = \delta_j X(t)$. To relate regularity properties of signals from the amplitude of their wavelet coefficients, it is necessary to use wavelets having a better frequency localization than a difference of Diracs [7]. We use a complex wavelet ψ having a Fourier transform $\hat{\psi}(\omega) = \int \psi(t) e^{-i\omega t} dt$ which is real, and whose energy is mostly concentrated at frequencies $\omega \in [\pi, 2\pi]$. It results that $\hat{\psi}_j(\omega) = \hat{\psi}(2^j \omega)$ is non-negligible mostly in $\omega \in [2^{-j}\pi, 2^{-j+1}\pi]$. We suppose that ψ has $m \geq 1$ vanishing moments, which means that $|\hat{\psi}(\omega)| = O(|\omega|^m)$ in the neighborhood of $\omega = 0$.

In the following we shall restrict the scales 2^j to dyadic scales, and hence j to integers. To guarantee that W is invertible and satisfies an energy conservation [19], we impose that ψ satisfies the following Littlewood-Paley equality

$$\forall \omega > 0, \quad \sum_{j=-\infty}^{+\infty} |\hat{\psi}(2^j \omega)|^2 = 1. \quad (5)$$

The wavelet transform is computed up to a largest scale 2^J which is smaller than the signal size T . The signal lower frequencies in $[-2^{-J}\pi, 2^{-J}\pi]$ are captured by a low-pass filter $\phi_J(t)$ whose Fourier transform is

$$\hat{\phi}_J(\omega) = \left(\sum_{j=J+1}^{+\infty} |\hat{\psi}(2^j \omega)|^2 \right)^{1/2}. \quad (6)$$

One can verify that it has a unit integral $\int \phi_J(t) dt = 1$. To simplify notations, we write this low-pass filter as a last scale wavelet $\psi_{J+1} = \phi_J$, and $Wx(t, J+1) = x \star \psi_{J+1}(t)$. By applying the Parseval formula, we derive from (5) that for all x with $\|x\|^2 = \int |x(t)|^2 dt < \infty$

$$\|Wx\|^2 = \sum_{j=-\infty}^{J+1} \|x \star \psi_j\|^2 = \|x\|^2. \quad (7)$$

The wavelet transform W preserves the norm and is therefore invertible, with a stable inverse.

All numerical calculations below are performed with a complex Battle-Lemarié wavelet [20], [21], restricted to positive frequencies. Figure 1 shows the real and imaginary parts of ψ as well as its Fourier transform. It has $m = 4$ vanishing moments and satisfies the Littlewood-Paley equality (5). If the input signal is sampled at $t \in \mathbb{Z}$ then we can only compute wavelet coefficients for $2^j > 1$ and hence $j \geq 1$.

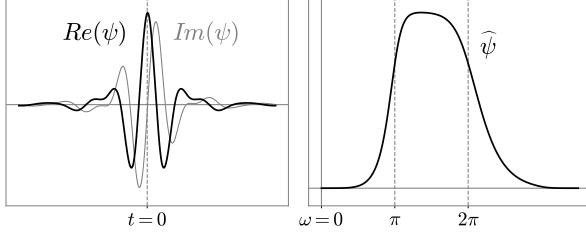


Fig. 1: Left: complex Battle-Lemarié wavelet $\psi(t)$ as a function of t . Right: Fourier transform $\hat{\psi}(\omega)$ as a function of ω .

Properties of signal increments are extended to wavelet coefficients by observing that wavelet coefficients are obtained by filtering signal increments $\delta_j X(t) = X(t) - X(t - 2^j)$ with a dilated integrable filter:

$$X \star \psi_j(t) = \delta_j X \star \theta_j(t) \quad \text{where} \quad \theta_j(t) = 2^{-j} \theta(2^{-j}t), \quad (8)$$

with $\hat{\theta}(\omega) = \hat{\psi}(\omega) / (1 - e^{-i\omega})$ and $\int |\theta(t)| dt < \infty$.

If $\delta_j X(t)$ is stationary then (8) implies that $X \star \psi_j(t)$ is also stationary. If X is self-similar then Appendix A derives from (1) that

$$\forall \ell \geq 0, \quad \left\{ X \star \psi_j(t) \right\}_{j \leq J, t \leq T} \stackrel{d}{=} A_\ell \left\{ X \star \psi_{j-\ell}(2^{-\ell}t) \right\}_{j \leq J, t \leq T}. \quad (9)$$

Since $X \star \psi_j(t)$ is stationary, its marginal probability distribution for t fixed does not depend upon t . If X is self-similar then Appendix A derives from (2) that for all $q \in \mathbb{R}$ there exists c_q such that

$$\forall j, \quad \mathbb{E}\{|X \star \psi_j|^q\} = c_q 2^{j\zeta_q}. \quad (10)$$

If X is Gaussian then one can verify that ζ_q is linear in q [17]. If ζ_q is non-linear but a convex function of q , under appropriate hypotheses, the multifractal theory [7] proves that (10) specifies the pointwise Holder regularity of X , through a spectrum of singularity.

III. DEPENDENCIES ACROSS SCALES WITH JOINT WAVELET ENVELOPE CORRELATIONS

Marginal probability distributions of wavelet coefficients $X \star \psi_j(t)$ are not sufficient to build accurate models of multi-scale processes. It is also necessary to capture their dependencies across times and scales. Next section shows that wavelet coefficients are not correlated at different scales although they may be strongly dependent, because of phase cancellation effects. Dependencies are represented with correlations of wavelet coefficients whose phase is separated with a modulus non-linearity.

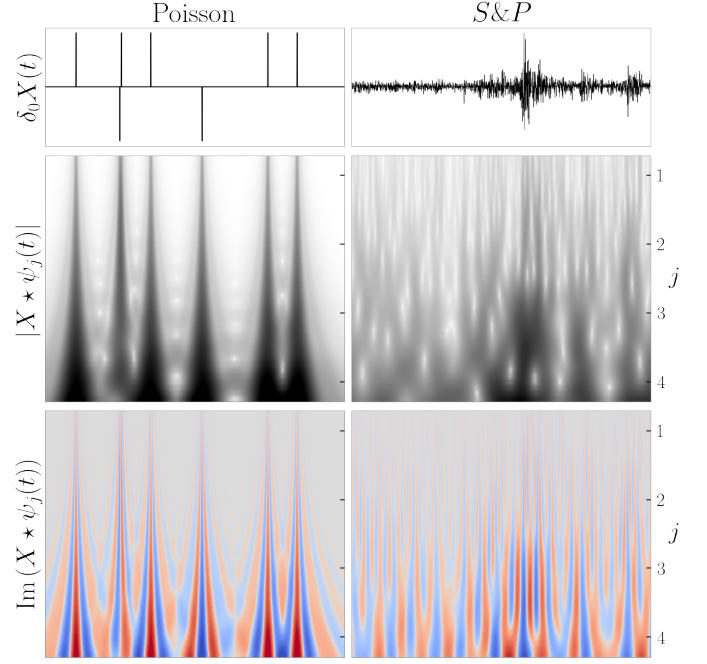


Fig. 2: Top: increments $\delta_0 X(t)$ of a signed Poisson process and the financial S&P daily increments from 03/01/2000 to 10/10/2018. Middle: wavelet envelopes $|X \star \psi_j(t)|$. The vertical axis corresponds to the log-scale index j . These envelopes have dependencies across scales produced by Diracs or bursts of activity. Bottom: imaginary part of $X \star \psi_j(t)$. It shows that coherent structures such as Dirac create correlation of phases across octaves, when j increases by 1 or more.

A. Wavelet Covariance

Non-Gaussian time-series have wavelet coefficients which are usually dependent across scales. Figure 2 shows the wavelet transform of S&P financial signal, and of a Poisson process whose increments have a random sign. They are calculated with the complex Battle-Lemarié wavelet. Diracs and bursts of activity in the financial signal create high amplitude wavelet coefficients, which propagate across scales. It induces strong dependencies between wavelet envelopes across scales. These dependencies also appear in the wavelet transform phase. Diracs produce high amplitude wavelet coefficients whose phase propagates regularly across octaves, when j increases by 1 or more. On the contrary, financial bursts of activity have a phase that is randomly modified from one octave to the next. Correlations when j increases by less than 1 are due to correlations between the wavelets themselves. To understand this correlation phenomenon, consider a localized pattern $f(t)$ in the neighborhood of $t = 0$, which is randomly translated to define $X(t) = f(t - U)$, where U is a random variable uniformly distributed in $[0, 1]$. Its wavelet coefficients $X \star \psi_j(t) = f \star \psi_j(t - U)$ are centered at $t = U$ at all scales 2^j , and are thus highly dependent. Their amplitude and phase are a signature of the translated pattern f .

In the following we restrict j to be an integer. The scale dependencies we just observed are not detected by the covariance of wavelet coefficients across scales. Since $\int \psi_j(t) dt = 0$

it results that $\mathbb{E}\{X \star \psi_j(t)\} = 0$, so the covariance coefficients define a τ dependent matrix

$$\tilde{C}_W(\tau; j, a) = \mathbb{E}\{X \star \psi_j(t) X \star \psi_{j-a}(t - 2^j \tau)^*\}.$$

Wavelet coefficients are not correlated across scales in the sense that

$$\tilde{C}_W(\tau; j, a) \approx 0$$

whenever $a \neq 0$. To verify this property, we rewrite this covariance from the power spectrum P_X of X which is well defined if X is stationary or has stationary increments. With a change of variables we verify that

$$\tilde{C}_W(\tau; j, a) = \frac{1}{2\pi} \int P_X(\omega) \hat{\psi}(2^j \omega) \hat{\psi}^*(2^{j-a} \omega) e^{i\tau 2^j \omega} d\omega. \quad (11)$$

It implies that $\tilde{C}_W(\tau; j, a) = 0$ if the support of $\hat{\psi}(\omega)$ and $\hat{\psi}(2^a \omega)$ do not overlap. This is typically the case if $|a| > 1$. When $|a| = 1$ wavelets have a small frequency overlap which produce small amplitude covariance coefficients, which appear in Figure 4a. If X is Gaussian then $X \star \psi_j$ and $X \star \psi_{j'}$ are jointly Gaussian and if they are uncorrelated then they are independent. However, this is typically not the case for non-Gaussian processes whose wavelet coefficients may be strongly dependant across scales, as shown in Figure 2.

Diagonal covariance values corresponding to $a = 0$ and $\tau = 0$ are written

$$\sigma^2(j) = \mathbb{E}\{|X \star \psi_j|^2\} = \frac{1}{2\pi} \int P_X(\omega) |\hat{\psi}(2^j \omega)|^2 d\omega. \quad (12)$$

This *wavelet spectrum* corresponds to the power spectrum $P_X(\omega)$ integrated over the frequency intervals $[2^{-j}\pi, 2^{-j+1}\pi]$, where $\hat{\psi}(2^j \omega)$ is mostly supported. If $P_X(\omega)$ is regular over such interval then (11) also shows that $\text{Cov}\{X \star \psi_j(t), X \star \psi_j(t - \tau)\}$ has a fast decay when $|\tau|$ increases. The wavelet covariance matrix is then a narrow band matrix which can be approximated by its diagonal. Figure 4a shows that this is verified for the S&P time-series. For $j = J+1$, $\sigma^2(J+1)$ is the power spectrum $P_X(\omega)$ integrated over $\omega \in [-2^{-J}\pi, 2^{-J+1}\pi]$. If it is finite, then the energy conservation (7) implies that

$$\mathbb{E}\{|X(t)|^2\} = \sum_{j=-\infty}^{J+1} \mathbb{E}\{|X \star \psi_j|^2\}.$$

B. Joint Wavelet Modulus Correlations Across Scales

Wavelet coefficients have a negligible correlation at different scales because wavelets are supported over different frequency intervals. To capture dependencies across scales by correlating wavelet coefficients, it is necessary to first realign their frequency support. This can be done by computing their amplitude with a modulus. This idea was first proposed by Portilla and Simoncelli [15]. The properties of wavelet transform envelopes have been studied to capture non-Gaussian characteristics of random processes [13], [22]. In the following we preserve phase information by correlating wavelet coefficients with and without phase. It provides information on dependencies across scales, that we shall adapt to the representation of multi-scale processes.

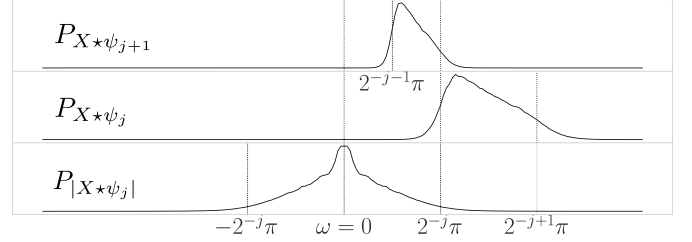


Fig. 3: Top: power spectrum of $X \star \psi_{j+1}$ for the S&P time-series. Middle: power spectrum of $X \star \psi_j$, mostly concentrated in $[2^{-j}\pi, 2^{-j+1}\pi]$. Bottom: the power spectrum of $|X \star \psi_j|$ is mostly concentrated in $[2^{-j}\pi, 2^{-j}\pi]$ and strongly overlaps with the power spectrum of $X \star \psi_{j+a}$ for $a > 0$.

1) *Non-zero Correlations by Phase Elimination:* Dependencies can appear across scale with a modulus, because it eliminates the phase which is responsible for the cancellation of correlations. Indeed, the power spectrum $P_X(\omega) |\hat{\psi}(2^j \omega)|^2$ of $X \star \psi_j$ has a support mostly concentrated in $[2^{-j}\pi, 2^{-j+1}\pi]$. The modulus eliminates the phase which oscillates at the center frequency $3 \times 2^{-j-1}\pi$. As a consequence, the power spectrum of $|X \star \psi_j|$ is centered at $\omega = 0$, and its energy is mostly concentrated in $[-2^{-j}\pi, 2^{-j}\pi]$ [13], [22]. This is illustrated in Figure 3. For a phase shift $a \neq 0$, we saw that wavelet coefficients $X \star \psi_j(t)$ and $X \star \psi_{j-a}(t - \tau)$ are essentially uncorrelated because their power spectra barely overlap.

Eliminating the phase with a modulus can introduce correlations across scales. Let us remind that the cross-spectrum $P_{Y,Z}(\omega)$ of two jointly stationary random variables $Y(t)$ and $Z(t)$ is the Fourier transform of their cross-correlation

$$\mathbb{E}\{Y(t)Z(t)^*\} = \frac{1}{2\pi} \int P_{Y,Z}(\omega) d\omega, \quad (13)$$

and the Cauchy-Schwarz inequality proves that

$$|P_{Y,Z}(\omega)|^2 \leq P_Y(\omega) P_Z(\omega). \quad (14)$$

Applied to $Y(t) = X \star \psi_j(t)$ and $Z(t) = |X \star \psi_{j-a}(t - \tau)|$ proves that they are uncorrelated if their power spectra do not overlap. This is nearly the case if $a < 0$. On the opposite, if $a \geq 0$ then their power spectrum overlap. It results that $|X \star \psi_j(t - \tau)|$ may be correlated with $X \star \psi_{j-a}(t)$. For any a , $|X \star \psi_j(t)|$ and $|X \star \psi_{j-a}(t - \tau)|$ may also be correlated because they have a power spectra which overlap since they are both centered at $\omega = 0$.

To express dependencies across scales, we propose to compute the joint second order moment of $(WX, |WX|)$ whose coefficients are $(X \star \psi_j(t), |X \star \psi_j(t)|)$, across all t, j . If X has stationary increments then $(\mathbb{E}\{WX\}, \mathbb{E}\{|WX|})$ does not depend upon time, but the low frequency coefficient may diverge if X is not stationary. We verify that $\mathbb{E}\{X \star \psi_j\} = 0$ for $j \leq J$ because $\int \psi_j(t) dt = 0$. If X is stationary then without loss of generality we shall suppose that $\mathbb{E}\{X(t)\} = 0$ by subtracting the mean, so we also have $\mathbb{E}\{X \star \psi_{J+1}\} = 0$ and hence $\mathbb{E}\{WX\} = 0$. On the contrary, the wavelet modulus $|WX|$ has non-zero averages $\mathbb{E}\{|X \star \psi_j(t)|\}$.

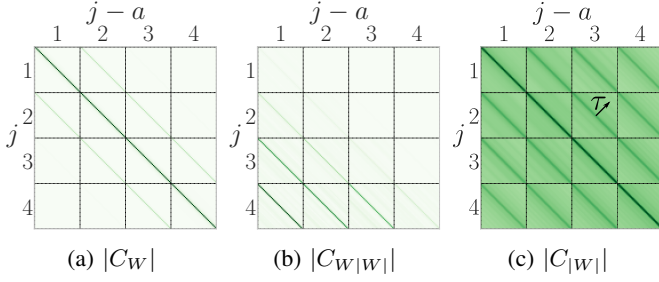


Fig. 4: Normalized correlation matrices C_W , $C_{W|W|}$ and $C_{|W|}$ for S&P signal. Each subblock is a Toeplitz correlation matrix along time $(t, t - 2^j \tau)$, for scales $(j, j - a)$ fixed, because of time stationarity. All correlation values are constant when j varies, which is a mark of wide-sense self-similarity.

The phased-modulus wavelet correlation on which we shall focus in the following is the normalized joint correlation matrix of $(WX, |WX|)$, which is composed of four submatrices

$$\begin{pmatrix} \mathbb{E}\{WXWX^*\} & \mathbb{E}\{WX|WX|^*\} \\ \mathbb{E}\{|WX|WX^*\}^* & \mathbb{E}\{|WX||WX|^*\} \end{pmatrix}$$

2) *Wavelet power spectrum*: The first matrix $\mathbb{E}\{WXWX^*\}$ is the wavelet correlation matrix. The previous section explains that we can approximate it by its diagonal values which define the wavelet spectrum $\sigma^2(j) = \mathbb{E}\{|X \star \psi_j|^2\}$. The normalized coefficients are

$$C_W(\tau; j, a) = \frac{\mathbb{E}\{X \star \psi_j(t) X \star \psi_{j-a}(t - 2^j \tau)^*\}}{\sigma(j) \sigma(j - a)}$$

3) *Phase-envelope Cross Spectrum*: The off-diagonal matrix $\mathbb{E}\{WX|WX|^*\}$ is a cross-correlation between complex wavelet coefficients and their envelope, that we shall call *phase-envelope correlation*. We normalize its coefficients by the wavelet spectrum

$$C_{W|W|}(\tau; j, a) = \frac{\mathbb{E}\{X \star \psi_j(t) |X \star \psi_{j-a}(t - 2^j \tau)|\}}{\sigma(j) \sigma(j - a)}.$$

Since $\mathbb{E}\{X \star \psi_j\} = 0$ these correlations are also covariance coefficients.

In Figure 4, the wavelet phase-envelope correlation $C_{W|W|}(\tau; j, a)$ is non-negligible for $a \geq 0$ and $\tau = 0$. Indeed, Figure 3 shows that the power spectrum of $X \star \psi_j$ and $|X \star \psi_{j-a}|$ have overlapping supports if $a \geq 0$, thus producing non-zero correlation coefficients

$$C_{W|W|}(0; j, a) = \frac{\mathbb{E}\{X \star \psi_j(t) |X \star \psi_{j-a}(t)|\}}{\sigma(j) \sigma(j - a)}. \quad (15)$$

For each step a along scales, according to (13) it gives a normalized cross-spectrum integral over the frequency interval $[2^{-j}\pi, 2^{-j+1}\pi]$ where the spectrum of $X \star \psi_j$ is concentrated. If this cross-spectrum is sufficiently regular then the covariance becomes negligible when the time-shift τ increases, as observed in Figure 4.

4) *Envelope Correlations*: The normalized correlation of the wavelet modulus $\mathbb{E}\{|WX|, |WX|\}$ is

$$C_{|W|}(\tau; j, a) = \frac{\mathbb{E}\{|X \star \psi_j(t)| |X \star \psi_{j-a}(t - 2^j \tau)|\}}{\sigma(j) \sigma(j - a)}.$$

A normalized covariance is obtained by subtracting the modulus means, which gives

$$C_{|W|}(\tau; j, a) = \frac{\mathbb{E}\{|X \star \psi_j(t)|\} \mathbb{E}\{|X \star \psi_{j-a}(t)|\}}{\sigma(j) \sigma(j - a)}. \quad (16)$$

Figure 4 shows that the normalized wavelet correlation is nearly a full matrix. Normalized covariances (16) are also a priori non-zero for all a , because the power spectra of $|X \star \psi_j|$ and $|X \star \psi_{j-a}|$ have overlapping supports. They may also remain non-negligible for large time translations by τ , because phase oscillations have been eliminated.

The maximum scale 2^j must be smaller than the signal support. If X is of size T then there are at most $\log_2 T$ scales j and scale shifts a . It results that there is at most $\log_2 T$ wavelet spectrum coefficients for C_W and $2^{-1} \log_2^2 T$ wavelet phase-envelope spectrum coefficients for $C_{W|W|}$. But since the number of time shifts τ is of the order of T , $C_{|W|}$ can have up to $T \log_2^2 T$ non-negligible coefficients. This correlation matrix is too large to be estimated accurately from a single realization of size T . Section V explains how to compute a low-dimensional approximation of this envelope correlation matrix, by applying a second wavelet transform.

5) *Non-Gaussian properties*: Phased and modulus wavelet correlations can be analyzed as particular cases of phase harmonic correlations introduced in [13]. It captures non-Gaussian properties proved in [22]. The following proposition proves that the existence of non-negligible wavelet modulus covariances across scales is a mark of non-Gaussianity.

Proposition 1. *If X is Gaussian and $\hat{\psi}_j \hat{\psi}_{j-a} = 0$ then for all τ*

$$C_{W|W|}(\tau; j, a) = 0$$

and

$$C_{|W|}(\tau; j, a) = \frac{E\{|X \star \psi_j(t)|\} E\{|X \star \psi_{j-a}(t)|\}}{\sigma(j) \sigma(j - a)}.$$

We indeed saw that if $\hat{\psi}_j \hat{\psi}_{j-a} = 0$ then $X \star \psi_j(t)$ and $X \star \psi_{j-a}(t - \tau)$ are uncorrelated. If X is Gaussian then they are also Gaussian and hence independent. Applying a modulus preserves this independence and thus produces covariance coefficients which remain zero, which proves the second equality. The condition $\hat{\psi}_j \hat{\psi}_{j-a} = 0$ is verified up to a very small error for $|a| > 1$. For $|a| = 1$, the supports of $\hat{\psi}_j$ and $\hat{\psi}_{j-a}$ overlap so the product is small but not zero.

Time-asymmetry is another form of non-Gaussianity, often produced by causality phenomena. Let R be the time reversal operator $Rx(t) = x(-t)$. A process X is said to be time-reversible if the probability distributions of RX and X are equal. Gaussian stationary processes are time-reversible. The following proposition shows that time-reversibility can be detected from phased correlation coefficients.

Proposition 2. *If X is time-reversible then C_W , $C_{W|W|}$ and $C_{|W|}$ have a Hermitian symmetry along τ :*

$$\begin{aligned} C_W(\tau; j, a) &= C_W(-\tau; j, a)^* \\ C_{W|W|}(\tau; j, a) &= C_{W|W|}(-\tau; j, a)^* \\ C_{|W|}(\tau; j, a) &= C_{|W|}(-\tau; j, a)^*. \end{aligned}$$

To prove this result, observe that $(RX) \star \psi_j(t) = X \star \psi_j(-t)^*$. We derive that applying R to X transforms $C_W(\tau; j, a)$ into $C_W(-\tau; j, a)^*$, $C_{W|W|}(\tau; j, a)$ into $C_{W|W|}(-\tau; j, a)^*$ and $C_{|W|}(\tau; j, a)$ into $C_{|W|}(-\tau; j, a)^*$. When X and RX have same distribution it proves the proposition. If phased correlations do not have the Hermitian symmetry specified by the proposition then X is not time-reversible, and hence non-Gaussian.

IV. WIDE-SENSE SELF-SIMILARITY

Self-similarity is defined in (1) and (9) as an equality over high-dimensional distributions, on increments or wavelet coefficients. Such properties cannot be verified numerically in high dimension. Section II gives necessary conditions over the marginals of increments and wavelet coefficients. They are simple to verify but relatively weak. The same difficulty appears to verify that a process is stationary. It can not be done numerically in high dimension. Marginal conditions impose that the marginal probability distribution of $X(t)$ does not depend upon t . It can be verified numerically but it is usually too weak. More powerful characterisations of stationarity are used for time-series, by imposing that $\mathbb{E}\{X(t)\}$ and the autocorrelation of X are invariant to time-shift. The process X is then said to be wide-sense stationary. We shall follow the same approach for self-similarity.

A wavelet transform introduces explicitly a scaling parameter 2^j . However, the correlations of wavelet coefficients WX vanish across scales, and thus can not be used directly to identify self-similarity across scales. We define a notion of wide-sense self-similarity as a translation and scaling invariance of the mean and correlation matrix of $(WX, |WX|)$.

Definition 3 (Wide-sense self-similarity). *A process X is wide-sense self-similar up to the scale 2^J if there exist $c_1, c_2, \zeta_1, \zeta_2$ such that for all $j \leq J$*

$$\mathbb{E}\{|X \star \psi_j(t)|\} = c_1 2^{j\zeta_1} \quad (17)$$

$$\mathbb{E}\{|X \star \psi_j(t)|^2\} = c_2 2^{j\zeta_2}. \quad (18)$$

and if for all $\tau, j \leq J, a$

$$C_W(\tau; j, a) = C_W(\tau; 0, a) \quad (19)$$

$$C_{W|W|}(\tau; j, a) = C_{W|W|}(\tau; 0, a) \quad (20)$$

$$C_{|W|}(\tau; j, a) = C_{|W|}(\tau; 0, a). \quad (21)$$

Similarly to marginal self-similarity (10), wide-sense self-similarity imposes the existence of scaling exponents ζ_q , but only for $q = 1$ and $q = 2$. The scaling exponent ζ_2 specifies the power spectrum decay. The ratio between first and second order moments is a sparsity measure

$$s^2(j) = \frac{\mathbb{E}\{|X \star \psi_j(t)|\}^2}{\sigma^2(j)} = c_s 2^{j\zeta_s} \leq 1, \quad (22)$$

where $c_s = c_1^2 c_2^{-1}$ and $\zeta_s = 2\zeta_1 - \zeta_2 \geq 0$. The lower $s^2(j)$ the sparser $X \star \psi_j(t)$. The exponent ζ_s is a sparsity rate which governs the increase of sparsity when the scale decreases. If X is Gaussian then $\zeta_s = 0$. If $\zeta_s > 0$ then the sparsity of $X \star \psi_j$ increases as j decreases. The constant c_s is a sparsity multiplicative factor. If X is Gaussian then $X \star \psi_j$ is also

Gaussian and one can verify that $c_s = \pi/4$, which is the ratio between first and second order moments of complex Gaussian random variables.

Wide-sense self-similarity also imposes that the correlation matrices C_W , $C_{W|W|}$ and $C_{|W|}$ are invariant to shifts by τ along time and by a along scales. This is a powerful second order condition, which is sufficient to reveal existence of complex self-similarity properties in time-series.

Theorem 4. *If X is self-similar in the sense of (9) then it is wide-sense self-similar.*

The theorem is proved in Appendix C. Processes such as fractional Brownian motion [1] or multifractal random walk [23] are self-similar and therefore wide-sense self-similar. Self-similarity cannot be verified numerically, whereas wide-sense self-similarity is a correlation property which can be estimated. Figure 4 shows that the S&P financial signal is wide-sense self-similar. Indeed $\log \mathbb{E}\{|X \star \psi_j|\}$ and $\log \mathbb{E}\{|X \star \psi_j|^2\}$ have a linear decay along j , and the normalized correlations $C_W, C_{W|W|}, C_{|W|}$ are constant along diagonals when j varies.

V. SCATTERING COVARIANCE

A time-series X of size T has a τ -dependent wavelet modulus correlation matrix $C_{|W|} = \mathbb{E}\{|WX||WX|\}$ which requires to estimate about $T \log_2^2 T$ correlation coefficients. Such a large number of coefficients cannot be estimated from a single realization of X . We thus introduce a low-dimensional approximation of this correlation matrix by applying a second wavelet transform, which defines a scattering transform. The resulting scattering covariance is nearly diagonal and can be estimated from a single realization.

A. Scattering Cross-Spectrum

The wavelet modulus $|WX|$ correlation is computed at all scales 2^j and for all scale shift a and time shift τ

$$C_{|W|}(\tau; j, a) = \frac{\mathbb{E}\{|X \star \psi_j(t)| |X \star \psi_{j-a}(t - \tau)|\}}{\sigma(j) \sigma(j - a)}. \quad (23)$$

Although $|X \star \psi_j(t)|$ and $|X \star \psi_{j-a}(t)|$ may have a long range correlation, one can build a low-dimensional representation of this matrix by applying a *second* wavelet transform, whose coefficients have a short range correlation at each scale. It amounts to compute a scattering transform, which iterates over wavelet transforms and modulus non-linearities [24].

Applying a second wavelet transform W on $|WX|$ defines $SX = W|WX|$, with

$$SX(t; j, k) := |X \star \psi_j| \star \psi_k(t). \quad (24)$$

It is non-negligible only if $k > j$. Indeed, the Fourier transform of $|X \star \psi_j|$ is mostly concentrated in $[-2^{-j}\pi, 2^{-j}\pi]$. If $k \leq j$ then it does not intersect the frequency interval $[2^{-k}\pi, 2^{-k+1}\pi]$ where the energy of $\widehat{\psi}_k$ is mostly concentrated, in which case $SX(t; j, k) \approx 0$.

At each scale 2^j , the scattering transform decomposes the wavelet spectrum. From the energy conservation (7) we derive that

$$\sum_{k=-\infty}^{J+1} \mathbb{E}\{|X \star \psi_j| \star \psi_k|^2\} = \mathbb{E}\{|X \star \psi_j|^2\}.$$

For discrete signals sampled at integers t , we have $k, j > 0$. Since $SX = W|WX|$, we have

$$\mathbb{E}\{SX SX^*\} = W \mathbb{E}\{|WX| |WX|\} W^*, \quad (25)$$

and it specifies $\mathbb{E}\{|WX| |WX|\}$ because W is invertible. The normalized scattering correlation $\mathbb{E}\{SX SX^*\}$ at $(t; j, k)$ and $(t - \tau; j - a, k')$ is

$$\frac{\mathbb{E}\{|X \star \psi_j| \star \psi_k(t) |X \star \psi_{j-a}| \star \psi_{k'}(t - \tau)^*\}}{\sigma(j) \sigma(j - a)}.$$

Since $\mathbb{E}\{|X \star \psi_j| \star \psi_k(t)\} = 0$, this correlation is a normalized covariance. Applying (13) to $Y(t) = |X \star \psi_j| \star \psi_k(t)$ and $Z = |X \star \psi_{j-a}| \star \psi_{k'}(t - \tau)$ shows that this covariance is negligible if $k \neq k'$ because the spectrum of Y and Z barely overlap. Indeed $\hat{\psi}_k$ and $\hat{\psi}_{k'}$ are concentrated over non-overlapping frequency intervals. These correlations have a fast decay along τ when the cross-spectrum of the envelopes is regular, and we shall only keep correlations for $\tau = 0$. These diagonal scattering covariances for $k = k' = j - b$ define a *scattering cross-spectrum*

$$C_S(j, a, b) = \frac{\mathbb{E}\{|X \star \psi_j| \star \psi_{j-b}(t) |X \star \psi_{j-a}| \star \psi_{j-b}(t)^*\}}{\sigma(j) \sigma(j - a)}. \quad (26)$$

Applying (13) to $Y = |X \star \psi_j| \star \psi_{j-b}$ and $Z = |X \star \psi_{j-a}| \star \psi_{j-b}$ shows that this covariance is non-negligible only if $b < 0$. Since ψ_{j-b} has a Fourier transform mostly supported in $[2^{-j+b}\pi, 2^{-j+b+1}\pi]$, these diagonal scattering covariances C_S give the cross-spectrum of $|X \star \psi_j|$ and $|X \star \psi_{j-a}|$ integrated over this frequency interval. These cross-spectra specify intermittency phenomena which appear when the envelope correlations are large across scales. If envelopes are uncorrelated in time across scales then $C_S(j, a, b)$ is nearly constant along b for j, a fixed. On the contrary, if $C_S(j, a, b)$ has a fast decay in b then it implies that the envelopes have long range correlations in time.

If X is of size T then there are at most $\log_2 T$ scales b . The time shift τ is replaced by the scale index b , which takes at most $\log_2 T$ values. Whereas $C_{|W|}$ is of size $T \log^2 T$ the diagonal scattering correlation C_S is much more parsimonious, at most of size $\log^3 T$.

The following proposition derives from Proposition (2) that the imaginary part of C_S captures time-asymmetry properties of X . The proof is in Appendix B.

Proposition 5. *If X is Gaussian and $\hat{\psi}_j \hat{\psi}_{j-a} = 0$ then*

$$C_S(j, a, b) = 0. \quad (27)$$

If X is time-reversible then for all j, a and b the imaginary part satisfies

$$\text{Im } C_S(j, a, b) = 0. \quad (28)$$

The following theorem proves that the self-similarity condition (21) on $C_{|W|}$ can be evaluated on non-zero scattering coefficients.

Theorem 6. *The scaling invariance (21) of $C_{|W|}$ implies that*

$$\forall j \leq J, \quad C_S(j, a, b) = C_S(0, a, b). \quad (29)$$

The theorem is proved in Appendix C. This condition on diagonal scattering coefficients is necessary and almost sufficient to guarantee the scaling invariance of $C_{|W|}$. To do so we would also need to impose an invariance condition on the off-diagonal coefficients of C_S but these coefficients have mostly a negligible amplitude. In the following, we shall thus systematically replace $C_{|W|}$ by the diagonal scattering correlation C_S and assess the scaling invariance (29). If C_S is scale invariant then it is specified by at most $\log_2^2 T$ coefficients.

B. Diagonal Scattering Covariance

A diagonal scattering covariance representation keeps the mean and diagonal spectral and cross-spectral coefficients of C_W , $C_{W|W|}$ and C_S . It is normalized for all $j \leq J + 1$ by the wavelet power spectrum

$$\sigma^2(j) = \mathbb{E}\{|X \star \psi_j|^2\}. \quad (30)$$

The wavelet mean is zero so we only keep the normalized mean of modulus wavelet coefficients, which define the sparsity factors

$$s^2(j) = \frac{\mathbb{E}\{|X \star \psi_j|^2\}}{\sigma^2(j)}. \quad (31)$$

The normalized diagonal wavelet phase-envelope cross-spectrum is

$$C_{W|W|}(0, j, a) = \frac{\mathbb{E}\{X \star \psi_j(t) |X \star \psi_{j-a}(t)|\}}{\sigma(j) \sigma(j - a)} \quad (32)$$

and the diagonal scattering cross-spectrum is

$$C_S(j, a, b) = \frac{\mathbb{E}\{|X \star \psi_j| \star \psi_{j-b}(t) |X \star \psi_{j-a}| \star \psi_{j-b}^*(t)\}}{\sigma(j) \sigma(j - a)}. \quad (33)$$

The diagonal scattering covariance is thus fully specified by

$$\mathcal{S} = \{\sigma^2, s^2, C_{W|W|}, C_S\}. \quad (34)$$

If X is known over T samples, then the maximum wavelet scale satisfies $2^J \leq T$ and \mathcal{S} is of dimension $5/2 + 7J/3 + J^2 + J^3/6$. We may chose $2^J < T$ if there exists an integrable scale 2^I such that $X(t)$ and $X(t - 2^I)$ are independent for all t . In this case X is stationary, and we set $2^J = 2^I$. Low-frequency scattering cross-spectrum are captured by the low-pass filter $\phi_J = \psi_{J+1}$ defined in (6), which are included in the diagonal scattering covariance.

A random process is wide-sense self-similar relatively to this scattering covariance if

- there exists $c_2, c_s, \zeta_2, \zeta_s$ such that for all $j \leq J$

$$\sigma^2(j) = c_2 2^{j\zeta_2} \quad \text{and} \quad s^2(j) = c_s 2^{j\zeta_s}$$

and

- $C_{W|W|}(0; j, a)$ and $C_S(j, a, b)$ do not depend upon j . They are then respectively equal to their average values

$$\overline{C}_{W|W|}(a) = \frac{1}{J - a} \sum_{j=a+1}^J C_{W|W|}(0; j, a) \quad (35)$$

$$\overline{C}_S(a, b) = \frac{1}{J + b - a} \sum_{j=a+1}^{J+b} C_S(j, a, b). \quad (36)$$

VI. NUMERICAL DASHBOARD FOR MULTI-SCALE PROCESSES

We show that the diagonal scattering covariance specifies intermittency, time-asymmetries and self-similarity properties of multi-scale processes. Next section studies standard mathematical models of multi-scale processes, and the following section considers numerical financial and turbulence time-series.

A. Models of self-similar processes

We consider Brownian motions, Poisson processes, multi-fractal random walks and Hawkes processes. To analyze their properties we display and analyze their diagonal scattering covariance, composed of

- $\sigma^2(j)$: wavelet power spectrum (30) in Figure 5a,
- $s^2(j)$: wavelet sparsity factor (31) in Figure 5b,
- $C_{W|W}(a)$: phase-envelope spectrum (32) in Figure 6.
- $C_S(a, b)$: scattering cross-spectrum (33) in Figure 7.

Over these models, expected values are computed with empirical averages over sufficiently long time-series to neglect estimation errors. Table I gives the power-law decay parameters of σ^2 and s^2 .

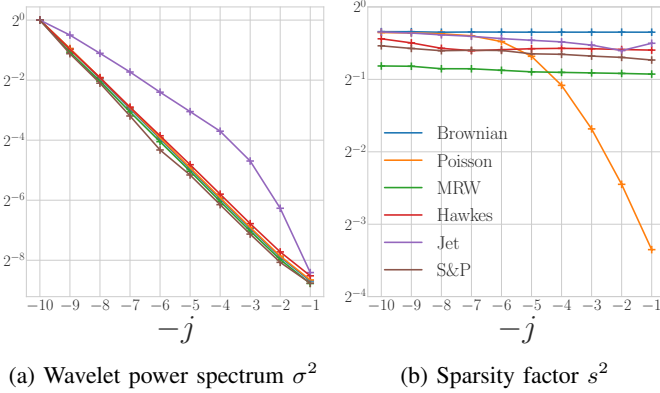


Fig. 5: (a) Power spectrum $\sigma^2(j)$ in (30) as a function of $-j$, which is a log frequency index. (b) Sparsity factor $s^2(j)$ in (31) as a function of $-j$. Each process is shown with a different color. Non-linear curves reveals absence of self-similarity for Poisson process and the turbulent jet at fine scales.

	Brown.	Poisson	MRW	Hawkes	Jet	S&P
ζ_2	1.0	1.0	1.0	1.0	0.66	1.0
c_s	0.79	×	0.66	0.65	0.67	0.61
ζ_s	0.00	×	0.016	0.013	0.025	0.016

TABLE I: Self-similarity parameters ζ_2, c_s, ζ_s , for different multi-scale processes. For the jet, ζ_2, c_s, ζ_s are given on the self-similar range.

a) *Fractional Brownian motion*: it is a Gaussian self-similar process, studied by Mandelbrot [1]. It has stationary increments and a generalized power spectrum $P_X(\omega) = c_2 |\omega|^{-\zeta_2-1}$. Computations are performed with $\zeta_2 = 1$, which corresponds to a standard Brownian motion. Wavelet sparsity coefficients have a power law decay with $c_s = \pi/4$ and $\zeta_s = 0$

in Table I, because it is a Gaussian process. Proposition 5 prove that $\overline{C}_{W|W}(a) \approx 0$ and $\overline{C}_S(a, b) \approx 0$ for $a > 0$, which is verified in Figure 6 and Figure 7. For $a = 0$, we also observe in Figure 7 that $\overline{C}_S(0, b)$ is constant, which shows that envelopes $|X \star \psi_j(t)|$ are uncorrelated at time increments which are sufficiently large relatively to the scale 2^j . As proved by Propositions 2 and 5, the phases of $C_{W|W}$ and C_S are zero in Figure 6 and 7, because a Gaussian process is time-reversible. Since Brownian motions are self-similar, the phase-envelope covariance $C_{W|W}$ and the scattering covariance C_S remain constant across scales 2^j .

b) *Poisson process*: it is a jump process having independent stationary increments. The number of jumps in an interval is proportional to the intensity λ . We further suppose that each jump is positive or negative with a probability 1/2. Its power spectrum has a power law decay with $\zeta_2 = 1$, but it is non-Gaussian and not self similar, which clearly appears in its diagonal scattering covariance. Figure 5b shows that $\log s^2(j)$ in (31) has a slope which varies as a function of $-j$. Indeed, if $2^j \ll \lambda^{-1}$ then [25] proves that $s^2(j) \sim 2^j$ because

$$\mathbb{E}\{|X \star \psi_j(t)|\}^2 \sim \lambda^2 2^{2j} \quad \text{and} \quad \mathbb{E}\{|X \star \psi_j(t)|^2\} \sim \lambda^2 2^j,$$

whereas if $2^j \gg \lambda^{-1}$ then $s^2(j) \sim 1$ because $X \star \psi_j(t)$ converges in distribution to a Gaussian white noise of variance $\lambda 2^j$, and hence

$$\mathbb{E}\{|X \star \psi_j(t)|\}^2 \sim \lambda 2^j \quad \text{and} \quad \mathbb{E}\{|X \star \psi_j(t)|^2\} \sim \lambda 2^j.$$

The non-self-similarity of Poisson process is also revealed by the large variations of $C_S(j, a, b)$ along j , which appears as large error bars in Figure 7.

c) *Multifractal Random Walk (MRW)*: it is a non-Gaussian self-similar process, whose increments have scaling exponents ζ_q in (2) that are quadratic in q . Increments are computed as a product of the increment $\delta_j B$ of a Brownian motion with a log-normal process

$$\delta_j X(t) = \delta_j B(t) e^{\Omega_j(t)}.$$

The Gaussian process $\Omega_j(t)$ has an autocorrelation with a slow logarithmic decay:

$$\text{Cov}\{\Omega_j(2^j t), \Omega_j(2^j t')\} = \lambda^2 \ln \theta(|t - t'|),$$

where θ decreases linearly and is specified in [23]. Since Ω_j is highly correlated in time, it creates wavelet envelopes that are also highly correlated in time with burst of activity. The parameter λ governs the intensity of this intermittency. If $\lambda = 0$ then the multifractal random walk is a Brownian motion. For MRW one can prove [23] that $\zeta_s = \lambda^2$, so Table I recovers the value $\lambda^2 = \zeta_s = 0.016$.

The scattering cross-spectrum $\overline{C}_S(a, b)$ gives the power spectrum of the cross-correlations of envelopes at two scales shifted by a , where b is a log-frequency index. The long range correlation of wavelet envelopes appears in Figure 7, which shows that $\overline{C}_S(a, b)$ has a power-law decay for each a .

A skewed multifractal random walk incorporates a time-asymmetry by imposing that increments in the past are correlated with the future volatility [26], in order to reflect the so-called leverage effect [27], [28]. This volatility is defined in

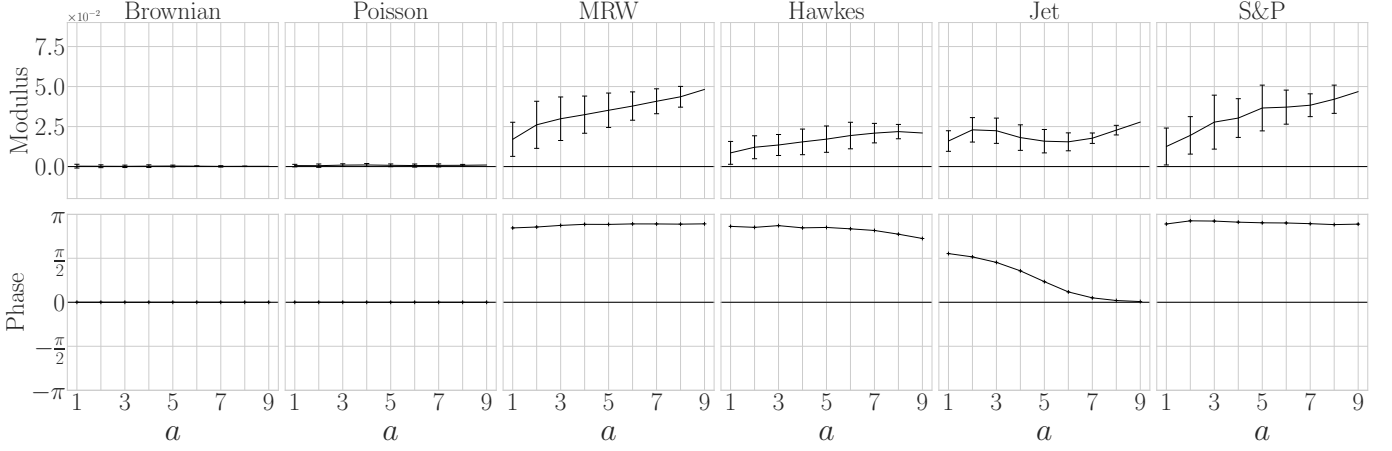


Fig. 6: Modulus and phase of the averaged phase-envelope cross-spectrum $\overline{C}_{W|W|}(a)$ (35). Error bars represent the mean-square variations of $C_{W|W|}(0; j, a)$ around $\overline{C}_{W|W|}(a)$. Non-zero phase coefficients reveal time-asymmetry.

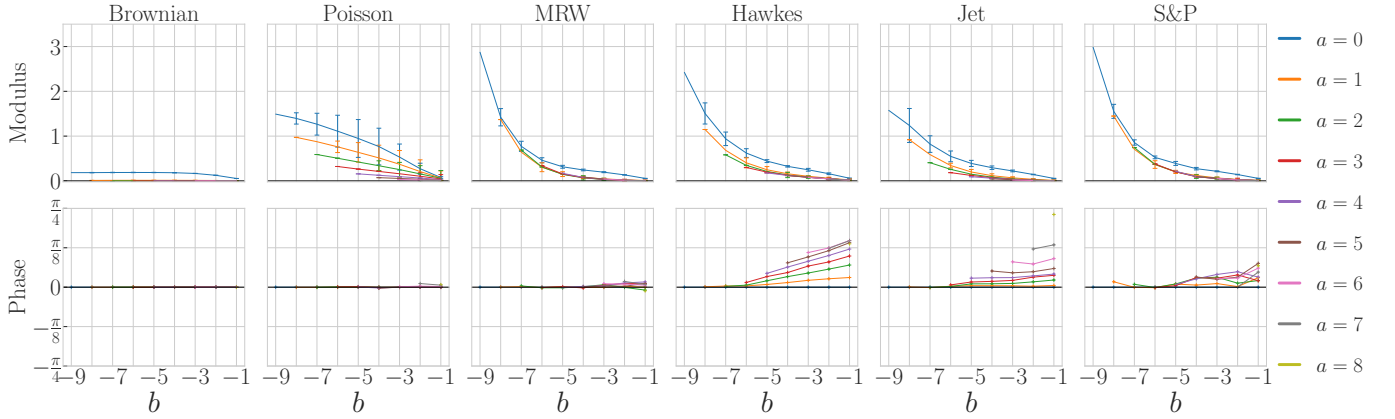


Fig. 7: Modulus and phase of the averaged scattering cross spectrum $\overline{C}_S(a, b)$ (36) as a function of b . The parameter b is a log-frequency. Each color curve corresponds to a different scale shift a . Error bars represent the mean-square variations of $C_S(j, a, b)$ around $\overline{C}_S(a, b)$. Non-zero phases reveal time-asymmetries of wavelet envelopes.

finance as the mean square average of increments over a fixed period of time. It amounts to replace the Gaussian process Ω_j by $\Omega_j - k \star \delta_j B$ where $k(t)$ is a strictly causal power-law convolution kernel. The faster K decreases the shorter the scale of asymmetry. Figure 6 shows $\overline{C}_{W|W|}(a)$ for skewed MRW. As expected from Proposition 2, this time-asymmetry is revealed by the non-zero phase of $\overline{C}_{W|W|}$, which implies that its imaginary part is also non-zero.

d) *Hawkes*: it is a non-homogeneous, causal self-excited point process [29], [30], where each jump is positive or negative with a probability 1/2. The jump intensity λ_t depends on the average of the past-jumps, with power-law decaying kernel h

$$\lambda_t = \lambda_\infty + h \star |dN|_t,$$

where dN_s is the signed jump measure and $h \star |dN|_t := \int_{-\infty}^t h(t-s)|dN_s|$. A linear feedback term $l \star dN_t$ can be added to account for correlation between past signed increments and future volatility.

A quadratic Hawkes model [31] introduces time-asymmetric envelope dependencies with a causal quadratic feedback of

kernel $k(t)$

$$\lambda_t = \lambda_\infty + h \star |dN|_t + l \star dN_t + |k \star dN_t|^2. \quad (37)$$

If $\int |h(t)| dt < 1$ then a quadratic Hawkes is stationary, and if $\int (|h(t)| + |k(t)|^2) dt < 1$ the mean intensity $\bar{\lambda}$ is finite [32]. In numerical simulation, as in [31] we set $h(t) \sim |t|^{-1.2}$, $g(t) \sim e^{-0.01|t|}$ and $k(t) \sim e^{-0.03|t|}$ with $\int (|h(t)| + |k(t)|^2) dt = 0.9$. As expected from Proposition 5, Figure 7 shows that for this quadratic Hawkes, $\overline{C}_S(a, b)$ has a non-zero phase which reveals its envelope time-asymmetry [33].

B. Analysis of multi-scale Time-Series

Brownian motions, multifractal random walks and Hawkes processes are used as models of multi-scale time-series, particularly in finance and turbulence [1], [18], [29], [34], [35]. The next two paragraphs analyze the scattering covariance of financial and turbulent time-series. Expected values are computed with time average estimators, which introduce an estimation error.

1) *Finance*: Finding stochastic models of financial time-series is important to compute the price of financial instruments which mitigate financial risks, such as options. A Brownian motion is a simple first order model, on which the Black and Scholes option pricing formula is based. However, many studies have shown strong deviations to Gaussianity, including the existence of burst of activity and crises. Multifractal random walks, Hawkes processes and rough volatility models are among the most popular models used to capture non-Gaussian properties of financial markets [30], [31], [34], [36]–[38]. We consider the American stock index S&P log-prices sampled over 5 minutes from January 2000 to October 2018. A standard preprocessing is performed and is described in Appendix D. The resulting signal has $T = 7.5 \cdot 10^5$ samples.

Figure 5 and Table I show that S&P has a wavelet spectrum decay exponent $\zeta_2 = 1$, which is the same as a Brownian motion. However, its sparsity factor $c_s = 0.61 \neq \pi/4$ and exponent $\zeta_s = 0.016 \neq 0$, which shows that this time-series is clearly not Gaussian. These values are matched by the MRW model, and by a Hawkes process with calibrated parameters.

The S&P phase-envelope spectrum $\bar{C}_{W|W|}$ in Figure 6 is similar to a skewed multifractal random walk (SMRW), with a strong time-asymmetry shown by a non-zero phase, related to the leverage effect [27], [28]. The amplitude of $|\bar{C}_S(a, b)|$ in Figure 7 is similar for the S&P and the MRW. However, the phase of $\bar{C}_S(a, b)$ is non-zero for the S&P, which proves that wavelet envelopes are also asymmetric in time. This is not well captured by the SMRW model. Such an effect is referred to the Zumbach effect in finance, which can be explained from causal agent reactions to past trends [31], [33], [37]. Such an envelope time-asymmetry appears in the quadratic Hawkes model, but $|\bar{C}_S(a, b)|$ has different variations along the a direction for S&P and for the Hawkes model, presumably because of our choice of an exponentially decaying kernel $k(t)$ (which was calibrated on intraday data only).

This analysis of the scattering covariance shows that none of these mathematical models fully capture all statistical properties of the S&P time-series.

Financial signals are often believed to be self-similar. We can estimate whether the S&P satisfies the wide-sense self-similarity properties of Definition 3. The wavelet spectrum and sparsity factors in Figure 5 do indeed have a power law decay. Wide-sense self-similarity also imposes that $C_{W|W|}(0; j, a)$ and $C_S(j, a, b)$ do not depend upon the scale j . Figures 6 and 7 display their mean-square variations along j as error bars. They are of the same order as the estimation variance of each coefficients. We thus conclude that S&P time-series has no significant deviation from wide-sense self-similarity.

2) *Turbulence*: Kolmogorov introduced in 1941 a self-similar Gaussian model of turbulence [39]–[41], with an asymptotic analysis of Navier-Stokes equations at high Reynolds numbers. This analysis predicts that the projection of the velocity field on a line is a stationary process whose power spectrum has a power-law decay with $\zeta_2 = 2/3$. However, turbulence time-series are highly non-Gaussian, and Kolmogorov’s initial theory was then refined to take into account intermittency and the presence of vortices [42], [43].

We study the scattering covariance of experimental veloc-

ity measurements along a single direction, measured over a turbulent gaseous helium jet at low temperature, with a high Reynolds number equal to 929 [44]. This time-series has $T = 3.5 \cdot 10^7$ samples and is thus much larger than the S&P time-series, providing more accurate estimators of the scattering covariance. The non-zero phase of $\bar{C}_{W|W|}(a)$ and $\bar{C}_S(a, b)$ in Figures 6 and 7 shows a time-asymmetry, which results from the directionality of the jet propulsion. The quadratic Hawkes provides the best model of $\bar{C}_S(a, b)$ but it fails to accurately represent $\bar{C}_{W|W|}(a)$.

It thus appears that none of the existing mathematical model provides accurate models of this turbulent time-series.

Turbulence time-series may be self-similar on a frequency range limited by the Reynolds number at low frequencies and by the fluid viscosity at high frequencies. The wavelet power spectrum and sparsity factors in Figure 5 are indeed self-similar up to the finest scale $j = 2$, which is the diffusion scale created by the fluid viscosity. The self-similarity error bars in Figure 6 and Figure 7 are of the same order as for the S&P. However, their amplitude is statistically significant in this case because this time-series is 50 times larger than the S&P time-series and the estimation variance is thus much smaller. It shows that this turbulent time-series has significant deviations from wide-sense self-similarity.

VII. MAXIMUM ENTROPY SCATTERING COVARIANCE MODELS

Brownian motions, multifractal random walks and Hawkes models are defined by a fixed number of parameters which does not depend upon their size T . They can be calibrated on data, but we saw they are typically too restrictive to capture all important properties of multi-scale time-series. On the other hand, neural network models [45], [46] have a considerable flexibility but they can not be trained from a single time-series because the number of parameters is much larger than T . Maximum entropy models from scattering covariances provide intermediate size models with about $\log^3 T/6$ parameters for a time-series of size T , which can thus be accurately estimated. We study the approximation of multi-scale time-series from such models. Next section briefly reviews the gradient descent algorithm introduced in [16] to sample maximum entropy models. Section VII-C shows that scattering covariance models are sufficiently flexible to approximate a wide range of mathematical models, as well as real financial and turbulence data.

A. Microcanonical set and sampling

Let \bar{x} be a realization of X of T samples. We write $\mathcal{S}\bar{x}$ the estimation of a diagonal scattering covariance (34), with a time averaged cross-correlation of wavelet and scattering coefficients of \bar{x} . A microcanonical set of width ϵ is the set of all x whose estimated scattering covariances have close values:

$$\Omega_\epsilon = \{x \in \mathbb{R}^T \mid \|\mathcal{S}x - \mathcal{S}\bar{x}\|^2 \leq \epsilon\}.$$

The width ϵ is adjusted so that each realization of X of size T is in Ω_ϵ , with high probability. The probability distribution of X is thus essentially supported in Ω_ϵ . A microcanonical

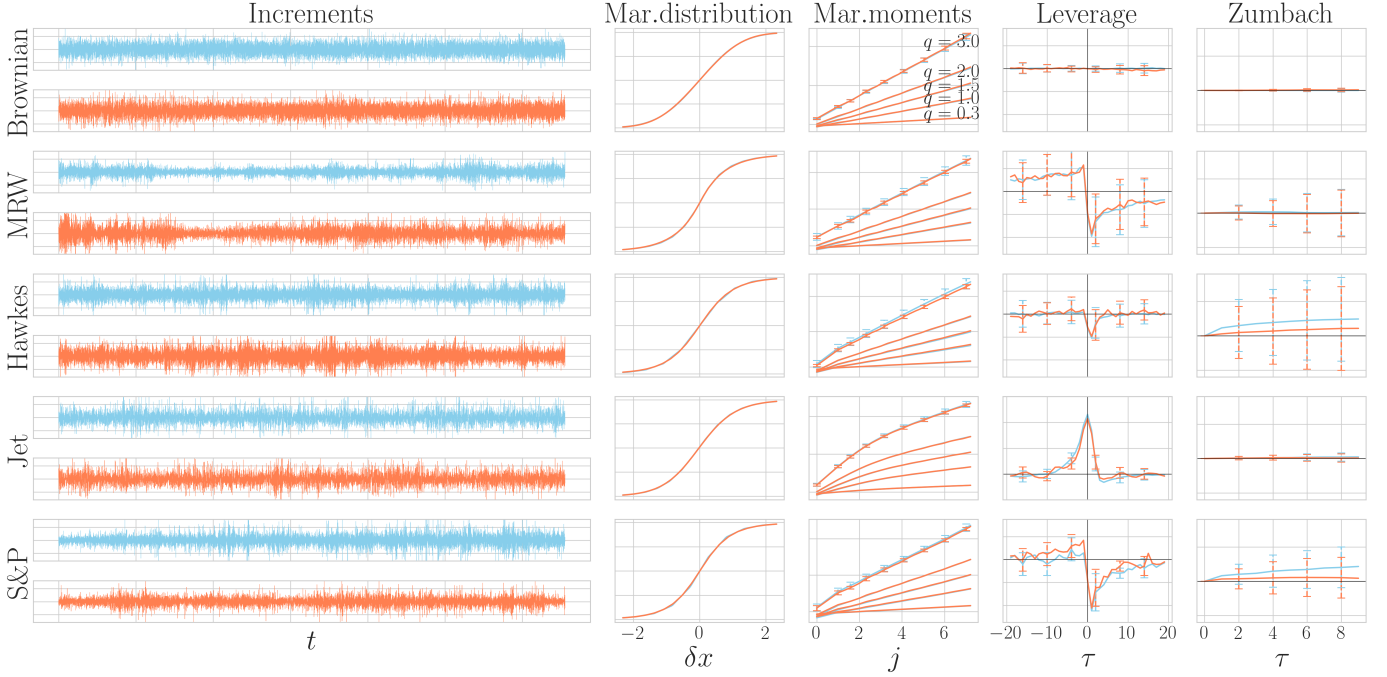


Fig. 8: Synthesis results. (Left) Increments $\delta_0 X(t)$ of original (blue) and generated (orange) time-series. (Right) Using the same color code: cumulative marginal distribution function $F(\delta x)$, marginal moments $\log \mathbb{E}\{|\delta_j X|^q\}$ as a function of j , leverage $\mathcal{L}_j(\tau)$ and Zumbach integral, for the Brownian, MRW, Hawkes, turbulent jet and S&P. In this last case, the value of j corresponds to one day. Error bars show the standard deviation for test moments of order greater than 3. While based on order 1 and order 2 moments, our model is able to capture higher order moments used to reveal scaling properties as well as time-asymmetries.

model is the probability distribution supported in Ω_ϵ which has a maximum entropy. Since Ω_ϵ is bounded, the microcanonical model has a uniform distribution over Ω_ϵ . The choice of the maximum scale 2^J amounts to define an integrable scale equal to 2^J , with low-frequency moments defined by the largest scale filter $\psi_{J+1} = \phi_J$. Indeed, the model imposes no constraints beyond the scale 2^J so the entropy maximisation produces coefficients which are nearly independent at distances much larger than 2^J .

Sampling a microcanonical realization amounts to randomly choose a signal in Ω_ϵ , with a uniform probability. We approximate this sampling with a gradient descent studied in [16]. It progressively transports a Gaussian white noise into a distribution supported in Ω_ϵ , with a gradient descent on $\ell(x) = \|\tilde{S}x - \tilde{S}\bar{x}\|^2$. We initialize x_0 to be a realization of a Gaussian white noise. At each iteration n , we update x_n with a gradient descent step

$$x_{n+1} = x_n - \eta \nabla \ell(x_n).$$

The gradient descent is implemented with the L-BFGS-B algorithm. It is proved in [16] that it converges to a measure which has the same symmetries as $\mathcal{S}x$, similarly to microcanonical measure. However, it is not guarantee to have a maximum entropy in Ω_ϵ .

B. Model Validation with Test Moments

Assessing the precision of a high-dimensional distribution model is an ill-defined problem. One may however find errors

by comparing test moments which are not used by the model, evaluated over the original time-series and on time-series generated by the model itself. Following [47], we describe test moments used in the finance literature to identify important differences relatively to Brownian motions. Figure 8 compares moment values obtained with a scattering covariance model and the original time-series. The following test moments are computed on increments $\delta_j X(t) = X(t) - X(t - 2^j)$ which are stationary. While our model considers dyadic scales $j \in \mathbb{Z}$, we consider all scales $2^j \in \mathbb{R}^+$ for test moments.

Cumulative distribution $F(\delta x)$ of increments $\delta_0 X(t) = X(t) - X(t - 1)$ at the finest scale.

Marginal high-order moments $\mathbb{E}\{|\delta_j X(t)|^q\}$ at all scales 2^j , for $0.3 \leq q \leq 3$. The multi-scale properties of these moments is reviewed in Section II-A.

Leverage moments measure asymmetric dependencies between past and future increments in finance [27], [28]. A leverage correlation for a time shift τ is an order 3 moment, at any scale 2^j :

$$\mathcal{L}_j(\tau) = \mathbb{E}\{\delta_j X(t - \tau) |\delta_j X(t)|^2\}.$$

If X has a time-reversible distribution then $\mathcal{L}_j(\tau) = -\mathcal{L}_j(-\tau)$. Results are shown in Figure 8 at an intermediate scale $2^j = 159$ that corresponds to the day in the case of S&P. The same scale is taken for all processes except for the Jet for which we take $2^j = 1$.

Zumbach moments evaluate the time-asymmetry of the volatility in finance [33], [37]. The volatility is the energy

of increments over a period of time of size 2^j

$$\Sigma_j^2(t) = 2^{-j} \sum_{u=t-2^j}^{t-1} |\delta_0 X(u)|^2.$$

A Zumbach moment for a time shift τ is an order 4 correlation at a scale 2^j

$$\mathcal{Z}_j(\tau) = \mathbb{E}\{|\delta_j X(t - \tau)|^2 \Sigma_j^2(t)\}.$$

If X is time-reversible then $\mathcal{Z}_j(-\tau) = \mathcal{Z}_j(\tau)$. To evaluate the time-asymmetry, Figure 8 shows $\int_0^t (\mathcal{Z}_j(s) - \mathcal{Z}_j(-s)) ds$ as a function of t for a scale $2^j = 159$, that corresponds to the day for S&P. This asymmetry coefficient on an order 4 moment is typically estimated with a large variance as we shall see.

C. Generation from Scattering Covariance Models

Figure 8 gives results of scattering covariance models computed from a single realization of a Brownian motion, a skewed MRW, a Hawkes process, a turbulence jet and the S&P financial signal. It displays realizations generated by these models and compares test moments. For financial and turbulence data, the syntheses recover signals of size $T = 7.10^5$ with models computed over $J = 11$ scales. The resulting scattering covariance model has 376 parameters.

Figure 8 shows that all test moments of order 2 or below are perfectly reproduced by scattering covariance models, for Brownian motion, MRW and Hawkes as well as for the turbulence jet and S&P financial data. Marginal moments of order $1/3 \leq q \leq 3$ are captured by our model on all processes, which is in accordance with the fact that the cdf are well reproduced.

For test moments of order 3 or 4, including the leverage and Zumbach effects that capture time-asymmetries, we represent the variance of estimators with an error bar, which is quite large for the Zumbach effect. Leverage is well captured for MRW, Hawkes, Jet, and remains within the estimation error bar for S&P. Zumbach integral estimations have a much larger variance. The main information is in the sign of this integral, when significant. This test moment is again reproduced on both Hawkes and S&P within the estimation error. Its high variance clearly shows the importance of using low order moments, even for time-asymmetries. Scattering covariance models reveal such non-Gaussian properties with a modulus and moments of order 1 and 2. In the case of the S&P, we believe that any remaining discrepancy for the Zumbach effect comes from our somewhat naive treatment of closing period during the night, see Appendix D.

VIII. CONCLUSION

Our proposed diagonal scattering covariance matrix gives an interpretable low-dimensional representation of processes having stationary increments. It captures their power spectrum, multi-scale sparsity, and the dependencies of wavelet coefficients phase and modulus across scales. Wide-sense self-similar signals have a scattering covariance which is invariant to scale shifts, and thus define a representation of even lower dimension.

This diagonal scattering covariance can be estimated from a single realization. We showed numerically that it reveals potential non-Gaussianity and self-similarity properties. This was demonstrated on mathematical multi-scale models such as fractional Brownian motions, multifractal random walks and Hawkes processes, but also of real time-series in finance and turbulence. Maximum entropy scattering covariance models capture essentially multi-scale dependency properties and can be efficiently sampled with a microcanonical approach.

Scattering covariance models are related to generative convolutional neural networks based on covariance matrices [48]. Similarly to a one-hidden layer convolutional neural network, it computes a cascade of two convolutions and a pointwise non-linearity. The network filters are wavelets which are not learned. It provides a much lower dimensional representations of random processes than usual deep convolutional neural networks, which is interpretable. However, it only applies to signals which are stationary or have stationary increments.

APPENDIX A

PROOF SELF-SIMILARITY IN DISTRIBUTION IMPLIES SELF-SIMILARITY OF MARGINAL MOMENTS.

Let X be a stationary process that is self-similar according to (1). For $q \in \mathbb{R}$, marginal moments are written $S(q, j) = \mathbb{E}\{|\delta_j X(t)|^q\}$. They do not depend upon t . For all $\ell \geq 0, j \leq J$, self-similarity implies that marginal distributions are equal: $\delta_j X(2^\ell t) \stackrel{d}{=} A_\ell \delta_{j-\ell} X(t)$. On order q moments, since A_ℓ is independent from X this yields

$$S(q, j) = \mathbb{E}\{A_\ell^q\} S(q, j - \ell).$$

Since the factors $(A_\ell)_\ell$ are log-infinitely divisible, for all $\ell_1, \ell_2 \geq 0$ $\mathbb{E}\{A_{\ell_1+\ell_2}^q\} = \mathbb{E}\{A_{\ell_1}^q\} \mathbb{E}\{A_{\ell_2}^q\}$. This implies that $\log \mathbb{E}\{A_\ell^q\}$ is linear in ℓ which means there exists ζ_q such that $\mathbb{E}\{A_\ell^q\} = 2^{j\zeta_q}$. By defining $\tilde{S}(q, j) = 2^{-j\zeta_q} S(q, j)$, we obtain $\tilde{S}(q, j) = \tilde{S}(q, j - \ell)$ for all $j \leq J, \ell \geq 0$, which implies that $\tilde{S}(q, j)$ is equal to a constant \tilde{c}_q which does not depend on j

$$S(q, j) = \mathbb{E}\{|\delta_j X(t)|^q\} = \tilde{c}_q 2^{j\zeta_q}.$$

Let us now establish the same property for wavelet coefficients. According to the self-similarity property (1), wavelet coefficients satisfies (9). Indeed, one has:

$$\begin{aligned} X \star \psi_j(2^\ell t) &= \delta_j X \star \theta_j(2^\ell t) \text{ thanks to (8)} \\ &= \delta_j X(2^\ell \cdot) \star \theta_{j-\ell}(t) \text{ as } \theta_j \text{ are dilated filters} \\ &\stackrel{d}{=} A_\ell \delta_{j-\ell} X \star \theta_{j-\ell}(t) \text{ by self-similarity (1)} \\ &= A_\ell X \star \psi_{j-\ell}(t) \text{ thanks to (8)} \end{aligned}$$

Replacing increments by wavelet filters ψ_j , we similarly prove that there exists c_q such that for the same ζ_q :

$$\mathbb{E}\{|X \star \psi_j(t)|^q\} = c_q 2^{j\zeta_q}.$$

APPENDIX B

PROOF OF PROPOSITION 5

Let X be a Gaussian stationary process and assume that $\hat{\psi}_j \hat{\psi}_{j-a} = 0$. Then for any τ , $X \star \psi_j(t)$ and $X \star \psi_{j-a}(t - \tau)$ are decorrelated because their power spectra do not overlap.

Since X is Gaussian these are also Gaussian. It implies that the processes $X \star \psi_j(t)$ and $X \star \psi_{j-a}(t)$ are independent. In particular, $|X \star \psi_j| \star \psi_{j-b}(t)$ and $|X \star \psi_{j-a}| \star \psi_{j-b}(t)$ are independent. Their correlation is thus zero and $C_S(j, a, b) = 0$.

Let X be a stationary time-reversible process. Thanks to proposition (2) we know that $C_{|W|}$ has the Hermitian symmetry: $C_{|W|}(\tau; j, a) = C_{|W|}(-\tau; j, a)^*$. We derive from (25) that the diagonal scattering correlations C_S satisfies:

$$C_S(j, a, b) = \int_{\tau} C_{|W|}(\cdot; j, a) \star \psi_{-b}(\tau) \psi_{-b}(\tau)^* d\tau.$$

With $Rx(t) = x(-t)$, the Hermitian symmetry of $C_{|W|}$ implies that

$$\begin{aligned} C_S(j, a, b) &= \int_{\tau} RC_{|W|}(\cdot; j, a)^* \star \psi_{-b}(\tau) \psi_{-b}(\tau)^* d\tau \\ &= \int_{\tau} C_{|W|}(\cdot; j, a)^* \star R\psi_{-b}(-\tau) \psi_{-b}(\tau)^* d\tau \\ &= \int_{\tau} C_{|W|}(\cdot; j, a)^* \star \psi_{-b}^*(-\tau) \psi_{-b}(\tau)^* d\tau \\ &= \int_{\tau} C_{|W|}(\cdot; j, a)^* \star \psi_{-b}^*(-\tau) \psi_{-b}(-\tau) d\tau \\ &= C_S^*(j, a, b) \end{aligned}$$

because $R\psi_{-b} = \psi_{-b}^*$. It proves that $\text{Im } C_S(j, a, b) = 0$.

APPENDIX C

PROOF SELF-SIMILARITY IN DISTRIBUTION IMPLIES WIDE-SENSE SELF-SIMILARITY

Let X be a process with stationary increments that is self-similar and thus satisfies (9). For $q = 1$ and $q = 2$, Appendix A proves that $\mathbb{E}\{|X \star \psi_j(t)|\} = c_1 2^{j\zeta_1}$ and

$$\sigma^2(j) = \mathbb{E}\{|X \star \psi_j(t)|^2\} = c_2 2^{j\zeta_2}, \quad (38)$$

which proves (17) and (18).

The equality in distribution (9) implies that for τ, j, a fixed we have

$$\begin{aligned} &(X \star \psi_j(t), X \star \psi_{j-a}(t - 2^j \tau)) \\ &\stackrel{d}{=} A_{\ell} (X \star \psi_{j-\ell}(2^{-\ell} t), X \star \psi_{j-a}(2^{-\ell} t - 2^{j-\ell} \tau)) \end{aligned}$$

Applying a modulus and computing an expected value gives

$$\begin{aligned} \mathbb{E}[|X \star \psi_j(t)| |X \star \psi_{j-a}(t - 2^j \tau)|] &= \\ 2^{\ell\zeta_2} \mathbb{E}[|X \star \psi_{j-\ell}(t)| |X \star \psi_{j-a-\ell}(t - 2^{j-\ell} \tau)|], \end{aligned}$$

because of stationarity and $\mathbb{E}\{A_{\ell}^2\} = 2^{\ell\zeta_2}$. Normalized correlations $C_{|W|}(\tau; j, a)$ are calculated by dividing by $\sigma(j)\sigma(j-a)$. It results from (38) that

$$2^{\ell\zeta_2} \sigma(j)^{-1} \sigma(j-a)^{-1} = \sigma(j-\ell)^{-1} \sigma(j-a-\ell)^{-1}$$

and hence

$$C_{|W|}(\tau; j, a) = C_{|W|}(\tau, j-\ell, a).$$

Taking $j = \ell$ proves (21). Equation (19) and (20) are obtained similarly.

APPENDIX D

FINANCIAL DATA PREPROCESSING

We use a standard preprocessing on S&P data which accounts for missing values, overnight period, intraday seasonality and tick effect. It is performed on 5min increments of S&P from January 3rd 2000 to October 10th 2018 which represents 751 116 values.

Missing values, 17 956 5min increments, are replaced by independent Gaussian values with zero mean and standard deviation observed at this time of the day.

Intraday seasonality is the fact that the volatility is larger at certain typical hours of the day: it is a non-stationary effect. It is removed by dividing 5min increments by the average volatility profile over all days.

The overnight period corresponds to the first bin at the beginning of each day. The corresponding increments are generally larger than other 5min increments. That again creates a non-stationarity effect that can be attenuated by dividing each overnight increment by their average volatility on all days.

Prices of S&P are present on a grid with certain tick size. Hence, 5min increments are discrete with many values equal to 0 or to plus/minus the tick size. This tick effect is present only for high-frequency increments and hence breaks the scale invariance property at high frequency. To remove it we apply a low-pass filter to X that amounts to a moving average on small windows of 15 minutes.

REFERENCES

- [1] B. B. Mandelbrot and J. W. Van Ness, "Fractional brownian motions, fractional noises and applications," *SIAM review*, vol. 10, no. 4, pp. 422–437, 1968.
- [2] B. B. Mandelbrot, "Multifractals and $1/f$ noise wild self-affinity in physics (1963–1976)."
- [3] —, *The fractal geometry of nature*. W. H. Freeman and Co., 1982.
- [4] E. Bacry, J.-F. Muzy, and A. Arneodo, "Singularity spectrum of fractal signals from wavelet analysis: Exact results," *Journal of statistical physics*, vol. 70, no. 3, pp. 635–674, 1993.
- [5] J.-F. Muzy, E. Bacry, and A. Arneodo, "The multifractal formalism revisited with wavelets," *International Journal of Bifurcation and Chaos*, vol. 4, no. 02, pp. 245–302, 1994.
- [6] P. Abry, P. Flandrin, M. S. Taqqu, and D. Veitch, "Wavelets for the analysis, estimation, and synthesis of scaling data," *Self-Similar Network Traffic and Performance Evaluation*, pp. 39–88, 2000.
- [7] S. Jaffard, "Wavelet techniques in multifractal analysis," PARIS UNIV (FRANCE), Tech. Rep., 2004.
- [8] S. Jaffard, B. Lashermes, and P. Abry, "Wavelet leaders in multifractal analysis," in *Wavelet analysis and applications*. Springer, 2006, pp. 201–246.
- [9] H. Wendt, S. G. Roux, S. Jaffard, and P. Abry, "Wavelet leaders and bootstrap for multifractal analysis of images," *Signal Processing*, vol. 89, no. 6, pp. 1100–1114, 2009.
- [10] R. Leonarduzzi, P. Abry, H. Wendt, S. Jaffard, and H. Touchette, "A generalized multifractal formalism for the estimation of nonconcave multifractal spectra," *IEEE Transactions on Signal Processing*, vol. 67, no. 1, pp. 110–119, 2018.
- [11] U. Frisch and G. Parisi, "Fully developed turbulence and intermittency," *Proceedings of the International Summer School on Turbulence and Predictability in Geophysical Fluid Dynamics and Climate Dynamics*, p. 84–88, 1985.
- [12] D. R. Brillinger, "An introduction to polyspectra," *The Annals of mathematical statistics*, pp. 1351–1374, 1965.
- [13] S. Mallat, S. Zhang, and G. Rochette, "Phase harmonic correlations and convolutional neural networks," *Information and Inference: A Journal of the IMA*, vol. 9, no. 3, pp. 721–747, 2020.
- [14] J. Bruna and S. Mallat, "Invariant scattering convolution networks," *IEEE transactions on pattern analysis and machine intelligence*, vol. 35, no. 8, pp. 1872–1886, 2013.

- [15] J. Portilla and E. P. Simoncelli, "A parametric texture model based on joint statistics of complex wavelet coefficients," *International journal of computer vision*, vol. 40, no. 1, pp. 49–70, 2000.
- [16] J. Bruna and S. Mallat, "Multiscale sparse microcanonical models," *Mathematical Statistics and Learning*, vol. 1, no. 3, pp. 257–315, 2019.
- [17] V. Pipiras and M. S. Taqqu, *Long-range dependence and self-similarity*. Cambridge university press, 2017, vol. 45.
- [18] B. B. Mandelbrot, A. J. Fisher, and L. E. Calvet, "A multifractal model of asset returns," 1997.
- [19] S. Mallat, *A wavelet tour of signal processing*. Elsevier, 1999.
- [20] G. Battle, "A block spin construction of ondelettes. part i: Lemarié functions," *Communications in Mathematical Physics*, vol. 110, no. 4, pp. 601–615, 1987.
- [21] P.-G. Lemarié, "Ondelettes à localisation exponentielle," *J. Math. Pures Appl.*, vol. 67, pp. 227–236, 1988.
- [22] S. Zhang and S. Mallat, "Maximum entropy models from phase harmonic covariances," *Applied and Computational Harmonic Analysis*, vol. 53, pp. 199–230, 2021.
- [23] E. Bacry, J. Delour, and J. F. Muzy, "Multifractal random walk," *Phys. Rev. E*, vol. 64, p. 026103, Jul 2001. [Online]. Available: <https://link.aps.org/doi/10.1103/PhysRevE.64.026103>
- [24] S. Mallat, "Group invariant scattering," *Communications on Pure and Applied Mathematics*, vol. 65, no. 10, pp. 1331–1398, 2012.
- [25] J. Bruna, S. Mallat, E. Bacry, J.-F. Muzy *et al.*, "Intermittent process analysis with scattering moments," *Annals of Statistics*, vol. 43, no. 1, pp. 323–351, 2015.
- [26] B. Pochart and J.-P. Bouchaud, "The skewed multifractal random walk with applications to option smiles," *Quantitative finance*, vol. 2, no. 4, p. 303, 2002.
- [27] G. Bekaert and G. Wu, "Asymmetric volatility and risk in equity markets," *The review of financial studies*, vol. 13, no. 1, pp. 1–42, 2000.
- [28] J.-P. Bouchaud, A. Matacz, and M. Potters, "Leverage effect in financial markets: The retarded volatility model," *Physical review letters*, vol. 87, no. 22, p. 228701, 2001.
- [29] E. Bacry and J.-F. Muzy, "Hawkes model for price and trades high-frequency dynamics," *Quantitative Finance*, vol. 14, no. 7, pp. 1147–1166, 2014.
- [30] E. Bacry, I. Mastromatteo, and J.-F. Muzy, "Hawkes processes in finance," *Market Microstructure and Liquidity*, vol. 1, no. 01, p. 1550005, 2015.
- [31] P. Blanc, J. Donier, and J.-P. Bouchaud, "Quadratic hawkes processes for financial prices," *Quantitative Finance*, vol. 17, no. 2, pp. 171–188, 2017.
- [32] C. Aubrun, M. Benzaquen, and J.-P. Bouchaud, "On hawkes processes with infinite mean intensity," *arXiv*!, p. 2112.14161, 2021.
- [33] G. Zumbach, "Time reversal invariance in finance," *Quantitative Finance*, vol. 9, no. 5, pp. 505–515, 2009.
- [34] E. Bacry, J. Delour, and J.-F. Muzy, "Modelling financial time series using multifractal random walks," *Physica A: statistical mechanics and its applications*, vol. 299, no. 1-2, pp. 84–92, 2001.
- [35] N. Mordant, J. Delour, E. L  veque, A. Arn  odo, and J.-F. Pinton, "Long time correlations in lagrangian dynamics: a key to intermittency in turbulence," *Physical review letters*, vol. 89, no. 25, p. 254502, 2002.
- [36] B. B. Mandelbrot, "The variation of certain speculative prices," *The Journal of Business*, vol. 36, no. 4, p. 394–419, 1963.
- [37] R. Chicheportiche and J.-P. Bouchaud, "The fine-structure of volatility feedback i: Multi-scale self-reflexivity," *Physica A: Statistical Mechanics and its Applications*, vol. 410, pp. 174–195, 2014.
- [38] J. Gatheral, T. Jaisson, and M. Rosenbaum, "Volatility is rough," *Quantitative finance*, vol. 18, no. 6, pp. 933–949, 2018.
- [39] A. N. Kolmogorov, "Dissipation of energy in the locally isotropic turbulence," in *Dokl. Akad. Nauk SSSR A*, vol. 32, 1941, pp. 16–18.
- [40] —, "On degeneration (decay) of isotropic turbulence in an incompressible viscous liquid," in *Dokl. Akad. Nauk SSSR*, vol. 31, 1 941, pp. 538–540.
- [41] —, "The local structure of turbulence in incompressible viscous fluid for very large reynolds numbers," *Cr Acad. Sci. URSS*, vol. 30, pp. 301–305, 1941.
- [42] —, "A refinement of previous hypotheses concerning the local structure of turbulence in a viscous incompressible fluid at high reynolds number," *Journal of Fluid Mechanics*, vol. 13, no. 1, p. 82–85, 1962.
- [43] U. Frisch, "From global scaling, a la kolmogorov, to local multifractal scaling in fully developed turbulence," *Proceedings of the Royal Society of London. Series A: Mathematical and Physical Sciences*, vol. 434, no. 1890, pp. 89–99, 1991.
- [44] O. Chanal, B. Chabaud, B. Castaing, and B. H  bral, "Intermittency in a turbulent low temperature gaseous helium jet," *The European Physical Journal B-Condensed Matter and Complex Systems*, vol. 17, no. 2, pp. 309–317, 2000.
- [45] A. v. d. Oord, S. Dieleman, H. Zen, K. Simonyan, O. Vinyals, A. Graves, N. Kalchbrenner, A. Senior, and K. Kavukcuoglu, "Wavenet: A generative model for raw audio," *arXiv preprint arXiv:1609.03499*, 2016.
- [46] F. Eckerli, "Generative adversarial networks in finance: an overview," *Available at SSRN 3864965*, 2021.
- [47] R. Leonarduzzi, G. Rochette, J.-P. Bouchaud, and S. Mallat, "Maximum-entropy scattering models for financial time series," in *ICASSP 2019-2019 IEEE International Conference on Acoustics, Speech and Signal Processing (ICASSP)*. IEEE, 2019, pp. 5496–5500.
- [48] L. Gatys, A. S. Ecker, and M. Bethge, "Texture synthesis using convolutional neural networks," *Advances in neural information processing systems*, vol. 28, 2015.